ACCEPTED FOR PUBLICATION IN Ap
Preprint typeset using LaTeX style emulateapj v. 14/09/00

DUSTY NUCLEAR DISKS AND FILAMENTS IN EARLY TYPE GALAXIES[a]

[a] BASED ON OBSERVATIONS WITH THE NASA/ESA *HUBBLE SPACE TELESCOPE*, OBTAINED AT THE SPACE TELESCOPE SCIENCE INSTITUTE, WHICH IS OPERATED BY THE ASSOCIATION OF UNIVERSITIES FOR RESEARCH IN ASTRONOMY, INC. UNDER NASA CONTRACT NO. NAS5-26555.

H. D. Tran, Z. Tsvetanov, H. C. Ford and J. Davies
Department of Physics and Astronomy, Johns Hopkins University, Baltimore, MD 21218
W. Jaffe
Leiden Observatory, P.O. Box 9513, 2300 RA Leiden, The Netherlands
AND
F. C. van den Bosch[1], A. Rest
Department of Astronomy, University of Washington, Seattle, WA 98195
Draft version February 27, 2001

ABSTRACT

We examine the dust properties of a nearby distance-limited sample of early type galaxies using the WFPC2 of the *Hubble Space Telescope*. Dust is detected in 29 out of 67 galaxies (43%), including 12 with small nuclear dusty disks. In a separate sample of 40 galaxies biased for the detection of dust by virtue of their detection in the *IRAS* 100 μm band, dust is found in $\sim 78\%$ of the galaxies, 15 of which contain dusty disks. In those galaxies with detectable dust, the apparent mass of the dust correlates with radio and far infrared luminosity, becoming more significant for systems with filamentary dust. A majority of *IRAS* and radio detections are also associated with dusty galaxies rather than dustless galaxies. This indicates that thermal emission from clumpy, filamentary dust is the main source of the far-IR radiation in early type galaxies. Dust in small disk-like morphology tends to be well aligned with the major axis of the host galaxies, while filamentary dust appears to be more randomly distributed with no preference for alignment with any major galactic structure. This suggests that, if the dusty disks and filaments have a common origin, the dust originates externally and requires time to dynamically relax and settle in the galaxy potential in the form of compact disks. More galaxies with visible dust than without dust display emission lines, indicative of ionized gas, although such nuclear activity does not show a preference for dusty disk over filamentary dust. There appears to be a weak relationship between the mass of the dusty disks and central velocity dispersion of the galaxy, suggesting a connection with a similar recently recognized relationship between the latter and the black hole mass.

Subject headings: galaxies: elliptical and lenticular — galaxies: ISM — ISM: dust, extinction

1. INTRODUCTION

Elliptical galaxies have often been viewed as old, uniform systems, with little gas, dust and activity. Through the years, ground-based and especially high spatial resolution imaging studies with the *Hubble Space Telescope* (*HST*) have rapidly changed that view (Sadler & Gerhard 1985; Véron-Cetty & Véron 1988; Forbes 1991; Goudfrooij et al. 1994; Ferrarese et al. 1994; Jaffe et al. 1994; van den Bosch et al. 1994; van Dokkum & Franx 1995; Lauer et al. 1995; Faber et al. 1997; Ferrari et al. 1999; Tomita et al. 2000). Based on these surveys, early-type galaxies are now known to commonly contain large amount of dust in various forms and sometimes complex structures. Of particular interest are the small ($r \sim 1''$, 200 pc) dusty nuclear disks that have been found in the centers of elliptical galaxies (see review by Ford et al. 1997). Their discovery and the ionized gas disks, associated with the dust, opened up a new means of efficiently measuring the central mass potentials, possibly of supermassive black holes (BH), residing in the centers of galaxies (Harms et al. 1994; Ferrarese et al. 1996; Macchetto et al. 1997; Bower et al. 1998; van der Marel & van den Bosch 1998; Ferrarese & Ford 1999; Verdoes Kleijn et al. 2000).

In this paper, we conduct a survey of two large samples of elliptical galaxies to study their dust properties and how they are related to other global properties of the parent galaxies as a whole. The main sample consists of E or S0 galaxies from the Lyon/Meudon Extragalactic Database (LEDA), selected to be nearby with $v < 3400$ km s^{-1}, and lying at galactic latitude $> 20^\circ$ to minimize Galactic extinction. Details of the sample selection and morphological and photometric properties of the galaxies are described in Rest et al. (2001) (hereafter Paper I). A total of 130 galaxies meet our criteria, out of which 67 galaxies were observed by *HST* using WFPC2 in snapshot mode with the F702W filter (R band). We shall refer to this sample as the "snapshot" sample in the rest of the paper.

In order to better assess the results derived from the snapshot sample, we also discuss where relevant a sample of galaxies selected for their 100 μm *IRAS* emission. The rational is that these galaxies are selected for their higher

[1] Present address: MPI fur Astrophysik, Karl Schwarzschild Str. 1, Postfach 1317, 85741 Garching, Germany.

far-IR (60 and 100 μm) emission, and thus are probably more likely to contain large amount of dust. The selection criteria are similar to those of the snapshot sample except that the galaxies are drawn from the *HST* archive, and with the additional criterion that a 100 μm *IRAS* detection exist with $\gtrsim 3\sigma$ significance. A total of 40 galaxies with *HST*/WFPC2 images was collected from the *HST* archive, and examined. Hereafter, we refer to this sample as the "IRAS" sample.

Our goal is to provide a reliable assessment of the frequency of dust and dusty disks in early-type galaxies and how their morphology, amount, and dynamics relate to the activity and other characteristics of the host galaxies. The main strength of our snapshot study is the large and unbiased sample of galaxies, all imaged at similar high resolution. This will allow us to make reliable statistical statements regarding their dust properties. Ultimately, we wish to use those with dusty nuclear disks as a probe of the central BH masses, and study how they are related to their environment. For consistency with Paper I, we use $H_o = 80$ km s^{-1} Mpc^{-1} throughout the paper.

2. ANALYSIS

2.1. *Dust Morphology and Mass*

Some general properties of galaxies in the snapshot sample are listed in Table 1. Paper I describes the observations and reduction of the images. We now describe our analysis of the galaxies with dust. Paper I reports the detection of dust in 29 galaxies, or 43% of the snapshot sample (the method of dust detection is outlined below). This is generally comparable to those reported by previous studies of early-type galaxies, which have shown the following detection rates of dust: Sadler & Gerhard (1985):$\sim$ 40%; Véron-Cetty & Véron (1988): 23%; Goudfrooij et al. (1994): 41%; van Dokkum & Franx (1995): 48%; Ferrari et al. (1999): $\sim$ 75%; Tomita et al. (2000): 56%. The large variation in the dust detection rates among different studies may be due to the different methods of counting detections, or the different resolutions and sensitivities of the observations. The ground-based CCD study of Véron-Cetty & Véron (1988), for example, includes only dust at the level of $\gtrsim 10^4$ $M_\odot$, effectively missing all the small nuclear dust disks, resulting in an abnormally low detection rate. The relatively high detection rate of Ferrari et al. (1999), on the other hand, may be due to higher sensitivity and lower detection threshold. Also, we note that the 85% dust detection rate found by van den Bosch et al. (1994) for galaxies in the Virgo cluster is considerably higher than those mentioned above. The reason for this is because they included galaxies with weakly distorted isophotes, in which the presence of dust was not directly visible by eye. In several cases, it later turned out that these distortions were not due to dust, but rather to defects in the CCD chips (so called "measles"). Van den Bosch et al. (1994) detected dust "by eye" in 5 out of 14 galaxies (36%), which is in good agreement with other studies.

For our sample, the morphology of the dust is grouped into two broad categories: filamentary and disky. Of these systems, 17 have only filamentary dust with no disks, 9 have well-defined dusty disks, and 3 show dust lying not only in a disk-like morphology but also in widespread extended filaments. See Table 2 for a summary of the dust morphology found in the sample. In Paper I, the level of filamentary dust is described in a purely qualitative way, with the simple scale I, II or III being assigned to denote the least to most dusty galaxies through visual inspection only. Class I represents small traces of dust that do not greatly affect the isophotal shape of the galaxy; class II and III denote large amounts of dust that prevent a meaningful analysis of the isophotes and luminosity profiles. Figures 1 and 2 show examples of some of the galaxies with dusty disks and filaments. In this paper, we follow Sadler & Gerhard (1985) and van Dokkum & Franx (1995) to estimate the mass of the dust present in each system. The dust mass is given by:

$$M_d = \langle A_V \rangle \Sigma \Gamma^{-1} \quad (1)$$

where $\langle A_V \rangle$ is the mean visual extinction in magnitudes, Σ is the surface area covered by the dust, and Γ is the extinction coefficient per unit mass. We adopt $\Gamma = 6 \times 10^{-6}$ mag kpc^2 $M_\odot{}^{-1}$ (van Dokkum & Franx 1995).

To obtain $\langle A_V \rangle$, we first determine the optical depth from the ratio of the calibrated image to the model of its surface brightness generated from an isophotal elliptical fit, using the IRAF task "ellipse" with the dusty features masked out. The optical depth in R is then $\tau = -ln(F_{obs}/F_{mod})$, where F_{obs} is the observed flux and F_{mod} is the modeled flux, and $A_R = 1.0857\tau$. Assuming a Galactic extinction law with $R_V = 3.1$, we have $A_V = 1.33 A_R$ (Cardelli, Clayton & Mathis 1989). In determining the mean visual extinction, we include all areas where $\tau \gtrsim 0.02$, which is the minimum detectable τ. Along with the estimated mass of the visible dust, Table 2 lists the morphologies of the dust features, the mean visual absorption, the position angle (PA) of the major axis of the dust feature, and the PA of the galaxy major axis. Table 2 shows that the range of dust mass values for our sample is comparable to that obtained by Goudfrooij & de Jong (1995) and van Dokkum & Franx (1995), typically 10^1–10^5 $M_\odot{}^2$. In Table 3, we show a comparison of the optically derived gas mass estimated by our study with those of previous works. For consistency, we consider only results obtained from similar *HST* observations by van Dokkum & Franx (1995) and Tomita et al. (2000). A gas-to-dust ratio of 130 is assumed for our study, and previous mass values have been converted using distances listed in Table 1. Although the number of objects in common between these studies are small, the mass estimates are in reasonable good agreement, given the uncertainty of ~ 0.5 in logarithmic scale (Tomita et al. 2000) typical for this type of dust mass determination. The agreement appears better with van Dokkum & Franx (1995), who used the same method as our study, than with Tomita et al. (2000), who used color excess, giving mass values that are a few times to one order of magnitude larger than ours.

Note that the dust mass estimated above relies on the simple assumption of a foreground screen in front of a background light. Any dust embedded within the galaxies or intermixed with stars cannot be estimated by this method. For example, using radiative transfer calculations, including scattering of photons into the line of sight,

[2] van Dokkum & Franx (1995) refer to the total $M_{gas} + M_{dust}$ as the dust mass, with $M_{gas}/M_{dust} = 130$.

FIG. 1.— Examples of dusty nuclear disks. NGC 4125 and NGC 5813 contain both disky and filamentary dust. Compass arrow shows the direction of north.

FIG. 2.— Examples of galaxies containing filamentary dust of various levels. Both ESO 437−15 and ESO 580−26 are classified as F3; NGC 4589 is an F2 galaxy and NGC 3377 is F1, displaying a single thin strain of dust in the upper left region.

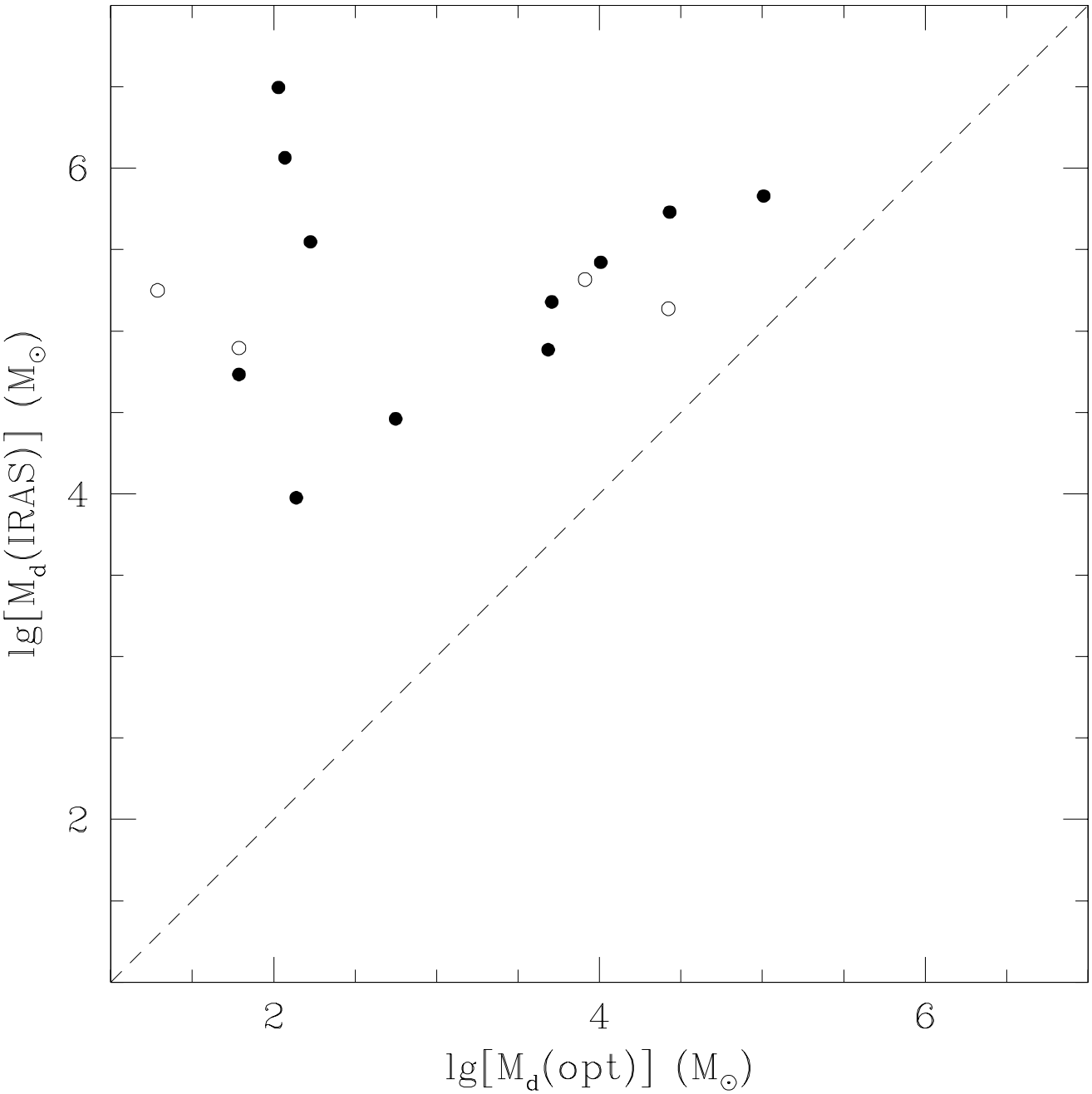

FIG. 3.— Relationship between the optically derived dust mass, $M_d(opt)$, and the dust mass estimated from $IRAS$ fluxes, $M_d(IRAS)$. Open circles denote dusty disks and filled circles denote filamentary dust. The dashed line represents $M_d(IRAS) = M_d(opt)$. As can be seen, for galaxies with both visual dust and $IRAS$ detections, $M_d(opt)$ is always lower than $M_d(IRAS)$ by 1–4 orders of magnitude.

Martel et al. (2000) have found that the mass estimated for the dusty disk in NGC 4261 is about one order of magnitude greater than that inferred from a foreground screen model. Furthermore, since we are fitting directly to the observed light, and it is impossible to mask out all faint dust features, we do not have a perfect model of the true underlying light. Thus the derived masses listed in Table 2 are always *lower* limits to the true mass.

Some of the missing non-clumpy, diffuse dust could be detected through its far-infrared radiation. This is confirmed by our estimates of the dust mass from the *IRAS* flux densities $M_d(IRAS)$. Following Goudfrooij & de Jong (1995), the dust mass is estimated from the *IRAS* flux through the formula:

$$M_d = 5.1 \times 10^{-11} S_\nu D^2 \lambda_\mu^4 (e^{1.44\times10^4/\lambda_\mu T_d} - 1)\ M_\odot \quad (2)$$

where S_ν is the *IRAS* flux density in mJy, D is distance in Mpc, and λ_μ is in μm. The dust temperature T_d is estimated from the color ratio S_{60}/S_{100}, according to the prescription of Kwan & Xie (1992), using an emissivity law that varies as λ^{-1}. For those galaxies where the color ratio S_{60}/S_{100} is not available, a representative color temperature of $T_d = 30$ K is assumed. We caution that the *IRAS* dust mass is very sensitive to such assumed parameters as grain size and temperature. Table 4 lists the radio and *IRAS* fluxes for those galaxies detected in the sample. The radio 1400 MHz flux densities are derived from the NRAO VLA Sky Survey (NVSS; Condon et al. 1998), and the *IRAS* fluxes are taken from Knapp et al. (1989), except for ESO 437-15, ESO 447-30, ESO 580-26, and NGC 2824, which are not included in their sample. For these galaxies, we measured their flux densities from the data scans by using the **apphot** package in IRAF and comparing the results to values in the *IRAS Faint Source Catalog* to derive scaling factors, which are similar to those of Knapp et al. (1989). As Figure 3 shows, for those galaxies with both *IRAS* detections and visibly detectable dust, the dust masses estimated from the *IRAS* fluxes, listed in Table 4, are $\sim$ 1–4 orders of magnitude greater than those derived from optical depth measurements of visual dust structures. This is consistent with earlier studies (Goudfrooij & de Jong 1995; de Koff et al. 2000).

2.2. *Correlation with Galaxy Properties*

Although the optically derived dust mass, $M_d(opt)$, always underestimates the true dust mass, we choose to use it in our analysis, since the *IRAS* derived dust mass, $M_d(IRAS)$ is unsuitable for any analysis relating to the far-IR properties. If derived in a consistent manner for the whole sample, $M_d(opt)$ should be a reliable representation of the dust mass. Moreover, some galaxies have no *IRAS* detections and yet dust is detected visually (see below). Presumably, most of the dust in these objects may be too cold ($\lesssim$ 20 K) to be detected by *IRAS* (Tsai & Mathews 1996; Merluzzi 1998). Figures 4 and 5 show the scatter plots of various properties of the snapshot sample galaxies versus dust mass. Table 5 summarizes the correlation coefficients for these plots. As can be seen, both the 60μm and 100μm luminosities are significantly correlated with dust mass. Furthermore, the correlation becomes stronger when the few systems with dusty disks are excluded. The only outliner is NGC 3065 whose IR fluxes are suspected to be contaminated with emission from NGC 3066, 3′ away (Knapp et al. 1989). This source is excluded from our statistical analysis. As Figure 4 and Table 5 also show, there appears to be no significant correlation between *IRAS* luminosities and absolute blue magnitudes of these galaxies. Turning to the radio property, Figure 5 and Table 5 show that the 1.4 GHz radio luminosity is also seen to follow a weak, but significant relationship with dust mass. However, in this case, the radio luminosity is also correlated with the optical luminosity of the galaxies, in agreement with Calvani, Fasano, & Franceschini (1989). This suggests that the $logL_{rad} - logM_d$ correlation may be largely a secondary effect of a more fundamental relationship between optical luminosity (and thus mass) and radio luminosity of the galaxy.

If one considers the radio detection rate, not constrained solely to those galaxies found to have dust, the correspondence of radio-emitting sources to the presence of dust is much stronger. Figure 6 and Table 6 present the detection rates of various properties for both the snapshot and *IRAS* samples. In the snapshot sample, only 8% of the galaxies without dust have radio detection, while 66% of the galaxies with dust do. Similarly, of the 26 galaxies in the snapshot sample with *IRAS* 100 μm detection, most (58%) are associated with dusty galaxies, a great majority of which are filamentary (Table 6). Since the galaxies are selected to be nearby ($\lesssim$ 40 Mpc), any distance effects are likely to be small. The overall rate of *IRAS* detection in the snapshot sample is 42%, consistent with those reported by Knapp et al. (1989) for E and S0 galaxies.

Turning to the *IRAS* sample listed in Table 7, about 3/4 (78%) of the galaxies contain dust (i.e., detection by eye from *HST* images) of some type, compared to only 43% for the snapshot sample. Since the *IRAS* sample is specifically selected for the detection of 100 μm emission, this suggests that the far-IR radiation largely arises from dust embedded throughout the galaxy.

As Figure 7 shows, there appears to be no correlation between the derived dust mass and absolute blue magnitude. This result is consistent with that of Goudfrooij & de Jong (1995) and van Dokkum & Franx (1995) but disagrees with Merluzzi (1998) and Ferrari et al. (1999). At first sight, this seems to suggest that there is little causal connection between the dust and the existing stellar population in the galaxy. However, if only the 12 galaxies with dusty disks are examined (open circles in Fig. 7), a clear relationship is evident between the dust mass and blue luminosity of the galaxies. The correlation between M_d and M_B is highly significant, with a Spearman rank coefficient of $r_s = -0.76$ ($p < 0.007$)[3]. NGC 4233 is an outliner, reducing the the significance of the correlation. Excluding NGC 4233 improves the correlation coefficient to $r_s = -0.88$ ($p < 0.0008$).

2.3. *Correlation with Velocity Dispersion*

The mass of the central BH in early type galaxies has been shown to be correlated with the bulge luminosity (and hence its mass; e.g., Kormendy & Richstone 1995;

[3] Since the correlation does not appear linear, we quote the Spearman rank coefficient here; a Pearson linear coefficient is given in Table 5 for comparison.

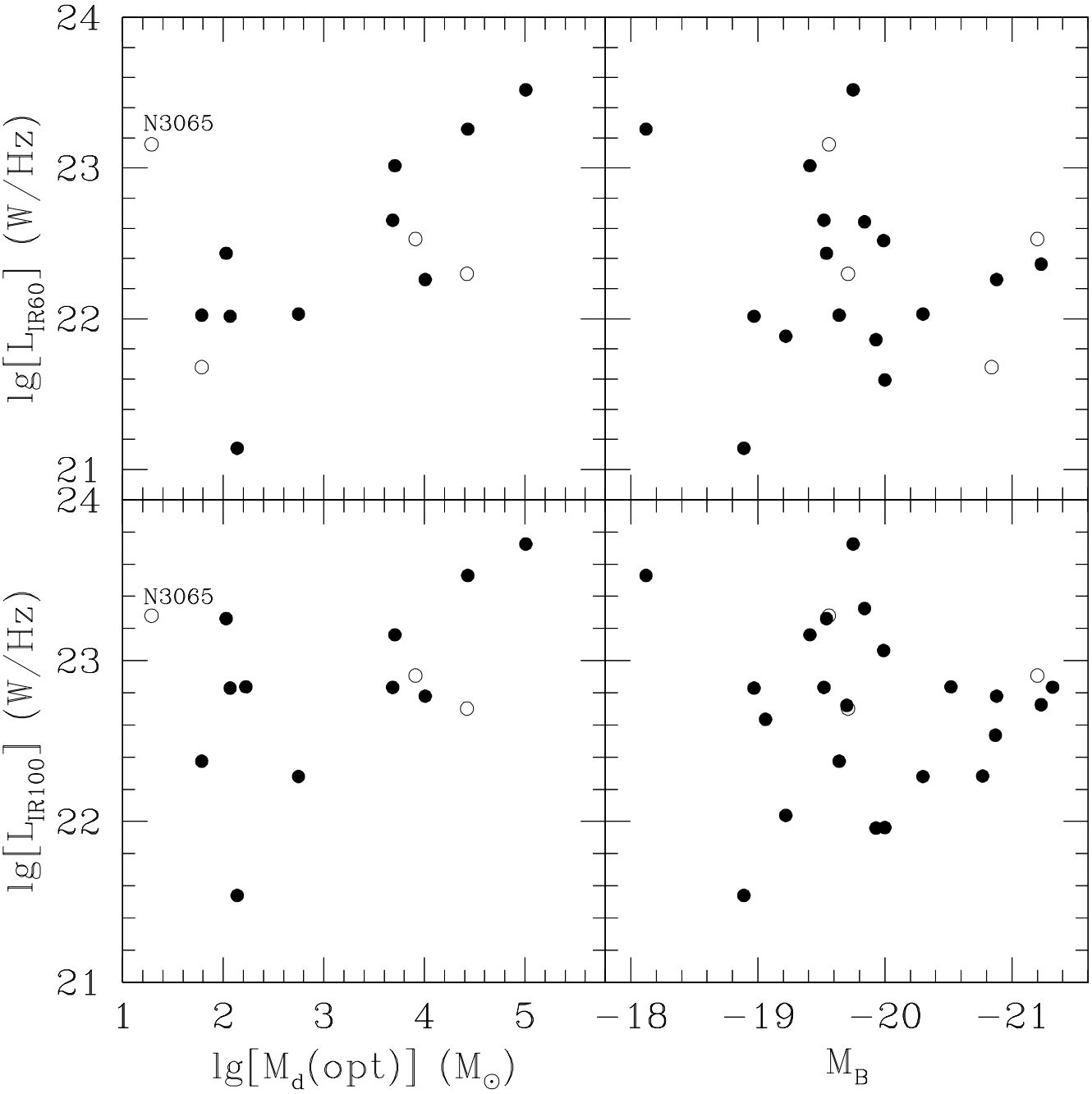

FIG. 4.— *IRAS* 60μm and 100μm luminosities versus absolute blue magnitude M_B and dust mass as determined from optical depth measurement M_d(opt). Symbols are as in Figure 3. There appears to be a significant correlation between *IRAS* luminosities and dust mass, especially when only filamentary dust systems are considered, but no correlation between *IRAS* luminosities and M_B. The only outliner is NGC 3065, whose *IRAS* fluxes are likely contaminated with emission from a nearby source.

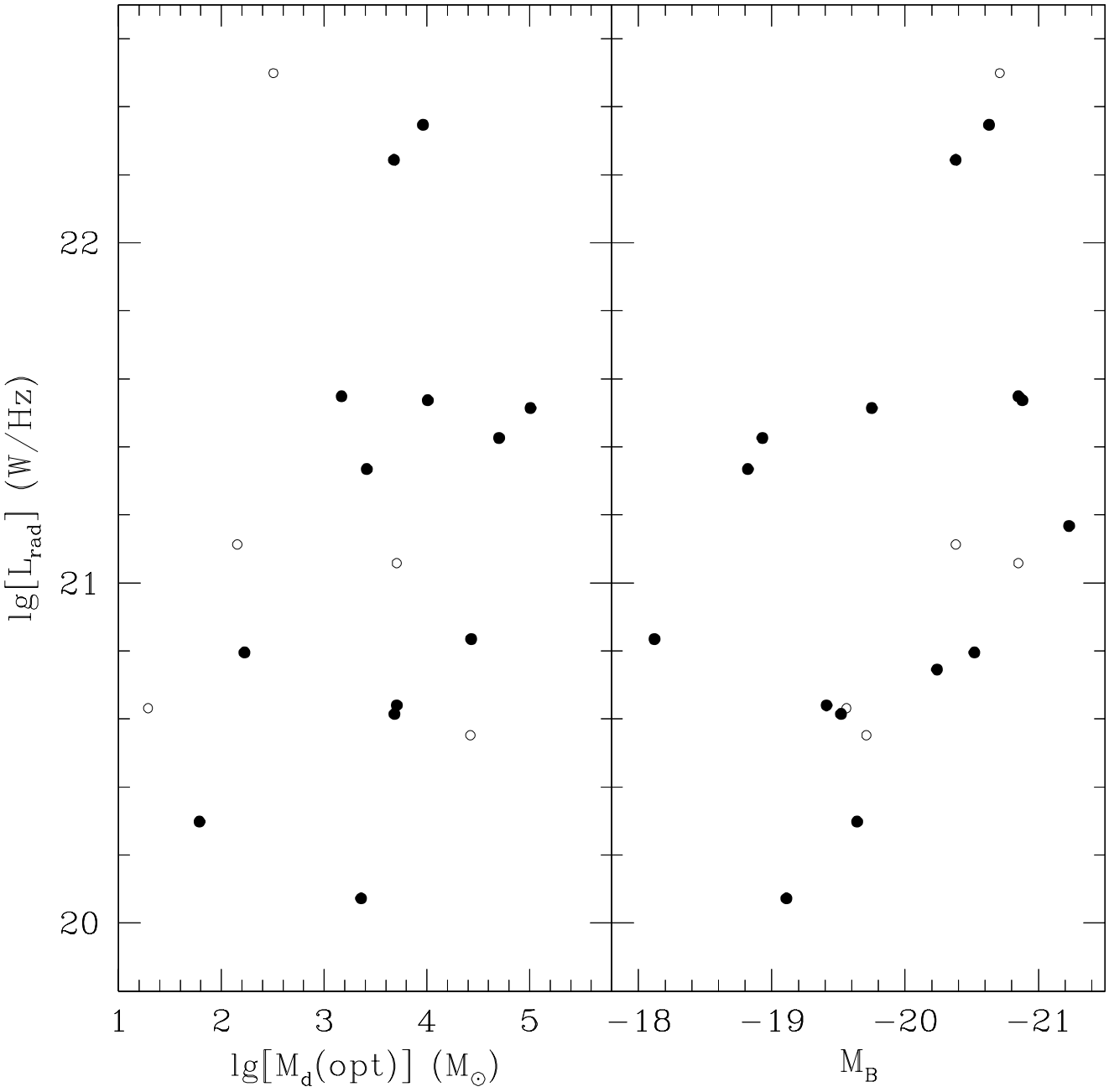

FIG. 5.— Radio luminosities at 1.4 GHz as detected by NVSS, L_{rad} versus dust mass and absolute blue magnitude. Symbols are as in Figure 3. There is a weak correlation between L_{rad} and M_d(opt), and a significant anticorrelation between L_{rad} and M_B.

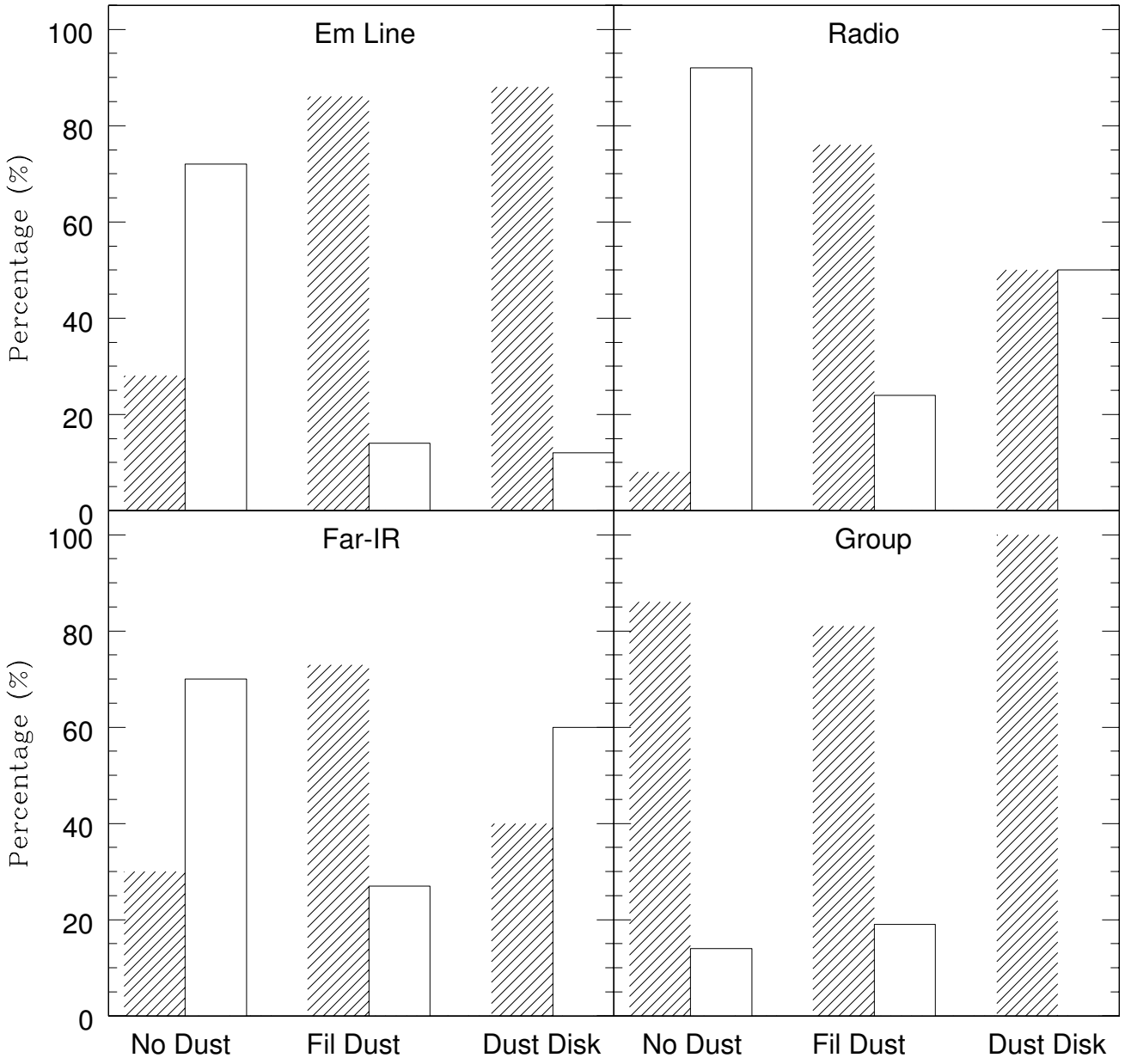

FIG. 6.— Detection rates of emission lines, radio 1.4 GHz emission, *IRAS* 60 μm and 100 μm emission, and being in group/cluster for three groups of galaxies in the snapshot sample: those with no dust, filamentary dust, and dusty disks. Shaded bar denotes detection, and empty bar denotes non-detection. Percentages are with respect to the number of galaxies in each group with available data. A much greater fraction of dusty galaxies has emission line, radio and *IRAS* detections than dustless galaxies. There is essentially no difference in the preference of being in group/cluster for galaxies with or without dust.

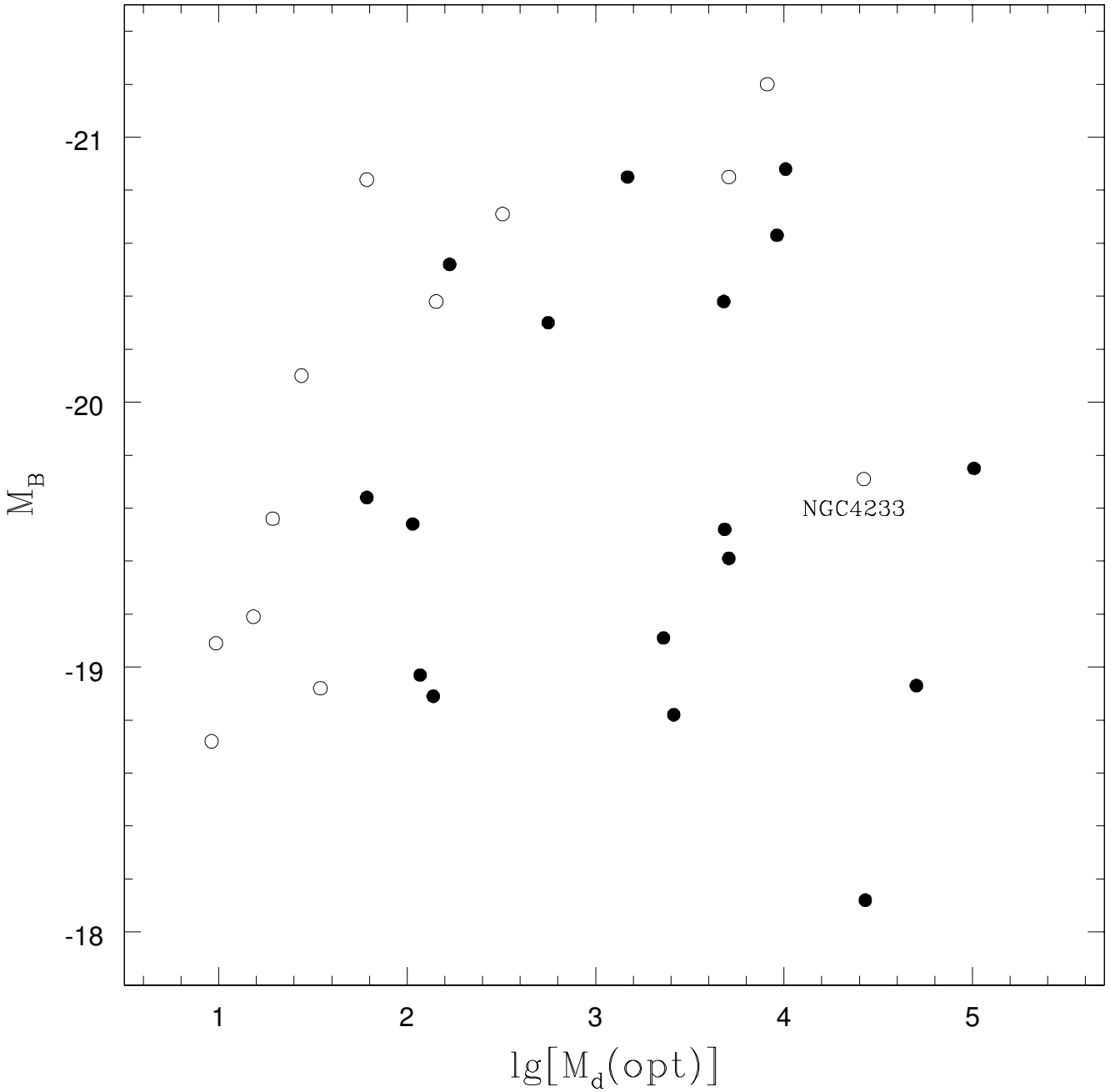

FIG. 7.— Absolute blue magnitude M_B versus optically derived dust mass M_d(opt). Symbols are as in Figure 3. No relationship exists when all systems are considered, but a significant correlation is evident for the dusty disk systems.

van der Marel 1999). Very recently, a much tighter correspondence has been shown between the BH mass and the velocity dispersion of the galaxy (Ferrarese & Merritt 2000; Gebhardt et al. 2000). In Figure 8 we show plots of the mass and diameter of the dusty disks versus the central velocity dispersion σ for both galaxies in the snapshot and *IRAS* samples. σ is the velocity dispersion taken from Davies et al. (1987) and McElroy (1995), and we have used distances derived from surface brightness fluctuation (SBF; e.g., Neilsen & Tsvetanov 2000) wherever possible. There appears to be a weak tendency for larger disks with higher dust mass to show higher velocity dispersion. However, the diagrams contain considerable scatters, and any correlation is very weak at best. Notable are the apparent "zones of avoidance" in the upper left and lower right areas of the graphs. A formal test shows that the M_d vs. σ plot has a correlation coefficient of $r = 0.45$ ($p[null] = 0.035$). Interestingly, in the disk size vs. σ diagram, the correlation seems to apply only for those galaxies whose dust disk diameter is $\lesssim 400$ pc. Those galaxies with very extended "disks", or more like lanes, such as NGC 5128 (Cen A), NGC 4697, NGC 4233, NGC 6861 and ESO 208-21 lie well above the trend line. Discarding these from the analysis, statistical test shows that the correlation has a coefficient of $r = 0.49$ ($p[null] = 0.022$).

If the correlation is real, it is interesting to speculate on the cause and implications of such a relationship. The more luminous galaxies with larger mass may be expected to contain more dust. Indeed, there is a strong relationship between dust mass and absolute magnitude for those galaxies with dusty disks (Fig. 7). The loose correlations between the disk size/mass and σ (Fig. 8) could be a direct consequence of a correlation between galaxy mass and σ, which has long been documented (Faber & Jackson 1976; Faber et al. 1987). The remarkable sharpness of the disks detected (Fig. 1) is also highly suggestive of some physical mechanism that acts to limit the size and shape of these disks. If so, the disk size/mass – σ relation indicates that such process is ultimately governed by the mass of the central BH.

2.4. *Origin of the Dust*

Clues to the origin of the dust can be glimpsed from a comparison of the PA between the major axis of the dust features and that of the galaxy. The isophotal PA of the galaxy's major axis is measured at $10''$, and listed in Table 2. Table 2 also lists the PA difference $|\Delta PA| = |PA_g - PA_d|$ between the two major axes. Figure 9 displays a distribution of the PA difference. As can be seen, the dusty nuclear disks have a high tendency to be aligned with the major axis of the host galaxies, nearly all within 10°, while the filamentary dust structures show a much lower tendency to align with their hosts. The former result is in agreement with that of Martel et al. (2000) for a sample of dusty disks in nearby 3CR elliptical galaxies. The median $|\Delta PA|$ for the dusty disks and filamentary dust are 5° and 23°, respectively. A K-S test confirms that the $|\Delta PA|$ distributions are significantly different, with only a 0.7% probability that they are drawn from the same parent population. This may suggest different origins for the disky and filamentary dust: internal for the dusty disk and external for filamentary dust. The presence of a correlation in Figure 7 for dusty disks but not for filamentary dust also seems to corroborate this. However, if both types of dust have a common origin, the most likely interpretation is that the dust comes from the outside and requires time to settle into well-organized disks. Again, the outliner is NGC 4233, which is the only galaxy with dusty "disk" that does show a misalignment ($\Delta PA = 52°$). This galaxy, however, happens to have very extended double dust lanes, rather than the more typical compact nuclear disk, perhaps suggesting that the dust has been acquired more recently and is still in the process of settling into a compact nuclear disk.

For those galaxies that have filamentary dust, the acquired dust has not yet had sufficient time to relax and achieve equilibrium in a "settled state". If the dust had arisen internally we would have expected a general alignment with the major dynamical axis of the galaxy. Our finding is consistent with that of van Dokkum & Franx (1995), who found a kinematic misalignment between the stars and the dust in a sample of early-type galaxies, suggesting that the two are not kinematically coupled, and thus have different origins. In a study of a sample of radio-loud active galaxies (the 3CR sample), de Koff et al. (2000) also find the dust in various forms similar to those seen here, and they suggest that these are also probably reflective of their different dynamical states. Previous studies have reached similar conclusion that the dust is external in origin (Kim 1989; Forbes 1991; Goudfrooij & de Jong 1995).

3. DISCUSSION

If the dust originated in a merger of two gas-rich disk galaxies (Barnes & Hernquist 1996, 1998), one might expect that the stars have not fully reached equilibrium either. However, no evidence for recent merger activity has been found in stars, even in the outer parts of the galaxy. This may suggest that the dust could arise from the tidal capture of gas from an encounter with a nearby galaxy. As a simple test of this hypothesis we have looked for any correlation between the amount of dust and local environment density of the galaxies in the snapshot sample. The group membership is taken from Garcia (1993), Huchra & Geller (1982) and Geller & Huchra (1983) and are listed in Table 1. As a rough measure of the size of the group we have also considered the group harmonic radius taken from Huchra & Geller (1982) and Geller & Huchra (1983). It is defined as $R_H = \frac{\pi V}{H_0} sin\{[N(N-1)\sum_{j<1}\sum_{i=1}\frac{1}{\theta_{ij}}]^{-1}\}$, where V is the mean velocity of the group, N is the number of group members, and θ_{ij} is the angular separation of the ith and jth group members. We show in Figure 10 the scatter plots of M_d versus N, R_H , and the number density of the group defined as $N/\frac{4}{3}\pi R_H^3$. As can be seen, there appears to be no correlation between the dust mass with any of these quantities.

As Table 6 and Figure 6 also show, there is virtually no difference between the extra-galactic environment of the two types of galaxies: dusty galaxies are no more likely to be found in groups or having close companions than dustless galaxies. These tests, therefore, fail to support an external origin for the dust. However, given other evidence for an external origin from this and previous studies, it may be possible for the dust to either be captured suf-

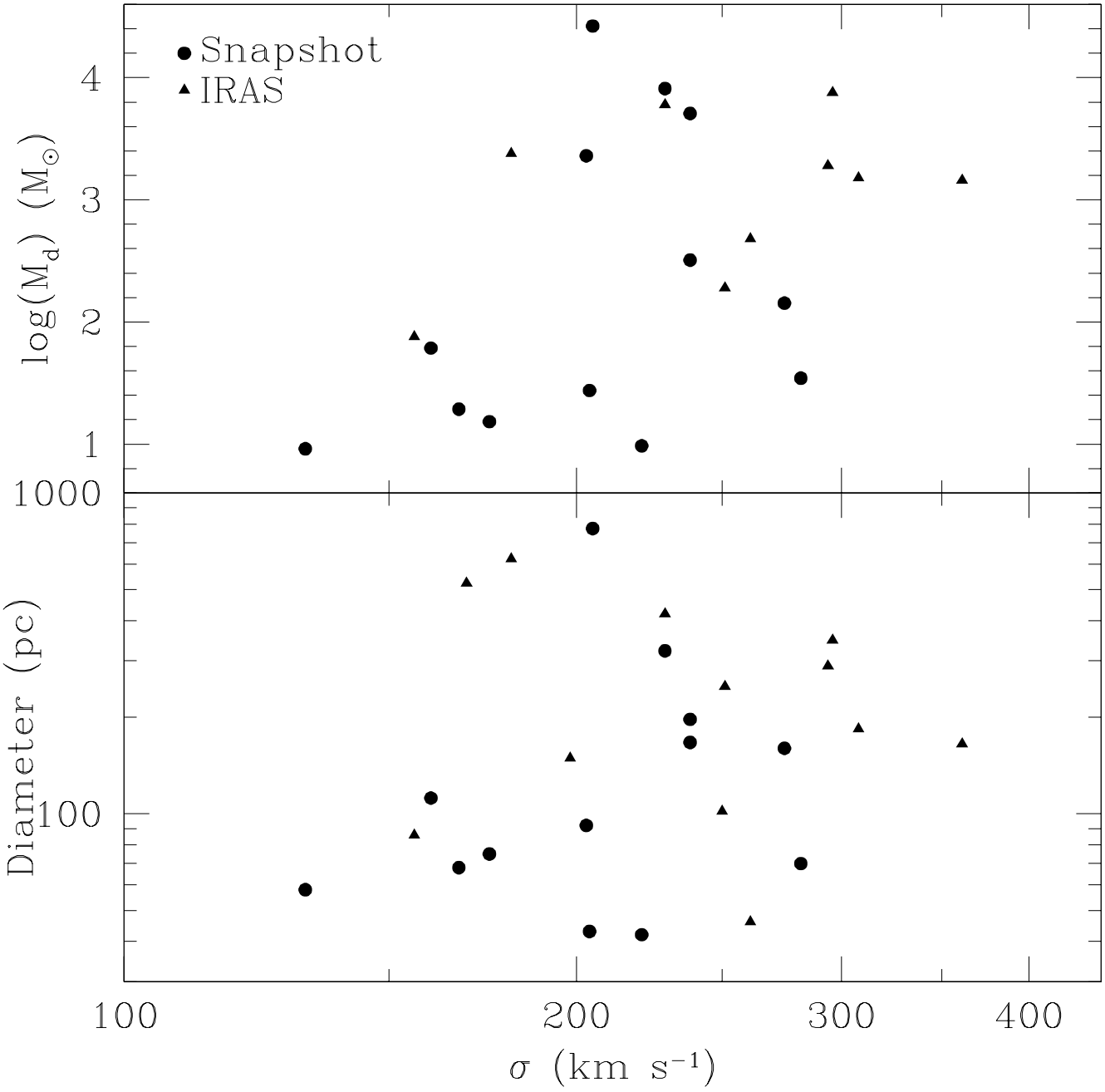

FIG. 8.— Relationship between the mass (*top*) or diameter, d (*bottom*) of the dusty disks and central velocity dispersion of the galaxy, σ. Filled circles denote galaxies from the snapshot sample, and filled triangles represent those from the *IRAS* sample. A weak but significant correlation is seen, especially for those systems with $d \lesssim 400$ pc.

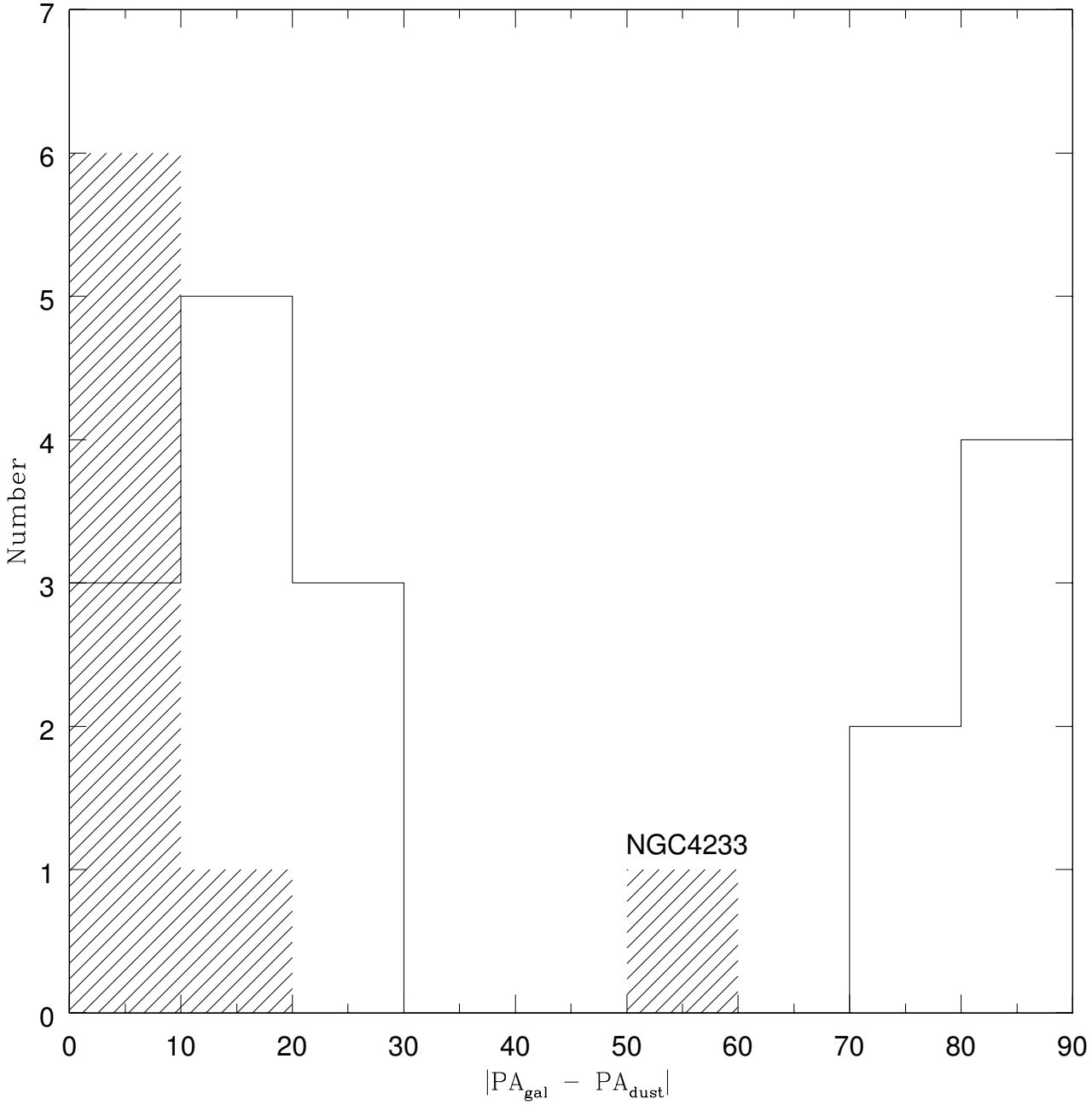

FIG. 9.— The distribution of the difference between the PA of the major axis of the galaxy and the PA of the major dust structure. Shaded histogram denotes dusty disks and empty histogram denotes filamentary dust systems. Systems with low inclinations (NGC 3065, NGC 4648, NGC 5017, NGC 5812) are excluded. Dusty disks are much more well aligned with the host galaxy than filamentary dust.

ficiently long ago that no signs of mergers or interactions are currently evident, or be acquired more recently but has an efficient way of losing angular momentum quickly. As shown by Tohline, Simonson, & Caldwell (1982) and Steiman-Cameron & Durisen (1988), the timescale that dissipative differential precession causes gas entering an elliptical galaxy to settle in a disk is fairly short ($\sim 10^9$ yrs). We note that an external origin, coupled with the $|\Delta PA|$ distribution in Figure 9, also suggests that elliptical galaxies are predominantly oblate (Tohline et al. 1982). The external or internal origin of the dust could be confirmed with a systematic spectroscopic study of a large and well-defined sample of galaxies with dust, such as that of the present study, to examine the dynamics and sense of rotation of the stars and gas. If approximately half of the disks are counter-rotating with respect to the stars, the dust most likely has an external origin. Such counter-rotating disks have been observed in a number of galaxies (Bertola & Corsini 1999; Caon, Macchetto & Pastoriza 2000), with a higher incidence in early-type galaxies (Kannappan & Fabricant 2000), providing support for the idea that these disks are products of galaxy interactions or mergers.

It has been shown that the presence of dust is closely associated with ionized gas in early-type galaxies (Caldwell 1984; Goudfrooij et al. 1994; Ferrari et al. 1999). The presence of ionized gas alone, however, does not establish the object as being a *bona fide* active galactic nuclei (AGN), with the excitation of the gas provided by photoionization from a central nonthermal continuum. Because active star forming regions are often associated with dust, in some of these systems, the gas ionization probably comes from circumnuclear starburst or high-velocity shocks and not a true active nucleus (i.e, gas-fed BH), although many are found to be LINERs (Table 1; many of which are believed to be low-luminosity AGNs). For the purpose of the following discussion, we shall take the presence of any emission line as a sign of galaxy activity.

We wish to see if ionized gas indicative of galactic activity is more reflective of not only dust, but dust in a small nuclear disk. That is, is it more likely for a galaxy to show emission lines when a dusty disk is present than when dust is filamentary in form or no dust is seen? It is natural to expect galaxies with dusty nuclear disks to show some level of nuclear activity because there is an ample gas supply from the disk to feed the central massive BH, if it is present. Furthermore, the closer the dust is to the nucleus, the more likely the connection is to the activity. To answer this question, we have searched the literature for observations of any line emission in the snapshot sample. Table 1 summarizes our results. Of the 67 galaxies in our snapshot sample, we found 43 with published observations establishing whether or not ionized gas is present. Our search indicates that 19 (86%) of the dusty galaxies do show line-emitting gas, compared to only 6 (28%) of the dustless galaxies. As §2.1 shows, however, if no dust is visually detected, it may not mean that it is truly free of dust; the dust could be in a diffuse, non-clumpy form that is not visibly apparent. Figure 6 indicates that the presence of line-emitting gas does not show any preference for galaxies with dust in the form of a small disk, or extended clumps/filaments. In fact, the incidence of emission lines is virtually identical ($\sim 87\%$) between the two groups. This indicates that emission line activity does show a strong preference for galaxies with *visibly detectable* dust, consistent with the finding by Caldwell (1984) and Tomita et al. (2000), but not necessarily in small nuclear disky form. Taken as a whole, emission lines occur in about 58% of the snapshot sample galaxies. This is consistent with Ho et al. (1997a), who found that the detection rate for emission line in E and S0 galaxies in a large, complete sample of nearby galaxies is 60%.

While most of the dusty disk galaxies in our sample have ionized gas, we have found at least a few without any signs of line emission (e.g., NGC 4406, NGC 4648). While this may indicate that the emission level is below the detection limit of the surveys, how the fuel is being fed to the central BH and the rate of accretion may be an important factor in determining the energy production and emission. Perhaps, a central massive BH may not have yet formed in some galaxies even though a dusty disk is present; alternatively, the BH is present but the accretion rate may not be high enough to ignite the activity: the absence of activity may be due to either a puny BH or an underfed massive one. For the two galaxies mentioned above, their velocity dispersions of order 240 km s^{-1} (McElroy 1995) suggest a black hole mass of $M_{BH} \approx 2 \times 10^8\ M_\odot$, quite typical of many early-type galaxies (Ferrarese & Merritt 2000; Gebhardt et al. 2000). Thus, their inactivity may most likely be due to a radiation inefficient mode of, or lack of, fuel accretion rather than a lack of a BH.

Further support for a lack of fuel transport comes from close examination of the central regions of dusty galaxies. Martini & Pogge (1999) examined WFPC2 images of the CfA sample of Seyfert 2 galaxies and found that the presence of nuclear spiral dust lanes within the inner 10-100 pc is nearly ubiquitous. Apparently, such dust spirals appear necessary in order for the gas to lose angular momentum and infall effectively into the supermassive BH, thereby producing real AGN activity. Although we were unable to produce color images for most of our galaxies since they were observed in only one band (F702W), examination of the optical depth images (see §2.1) revealed that nuclear dust spirals are not a common feature in our sample galaxies, appearing in only about four of 29 dusty galaxies. This is consistent with their lack of strong activity.

We showed in §2.2 that a significantly higher fraction of the galaxies with dust have detections in the radio. A survey of radio-loud early-type galaxies (Verdoes Kleijn et al. 1999) has shown that the incidence of dust is 89%, about twice as high as found in our snapshot sample of relatively benign, radio-quiet early-type galaxies (43%). Even in the *IRAS* sample, which is biased for the detection of dust, the dust detection rate (78%) is significantly lower than that of the radio-loud sample. However, the overall rates of radio and emission line detection are slightly higher than those in the snapshot sample (Table 6). Recently, Sparks et al. (2000) show that the detection rate of dust and dusty disks in nearby FR-I radio sources is nearly 100%. In 4 out of 5 cases where the galaxies are sufficiently nearby to allow a detailed look of the nuclei, Sparks et al. also report the presence of optical jets emanating perpendicular to face-on dust disks. These studies provide strong support for the idea that radio and nuclear activities are intimately linked

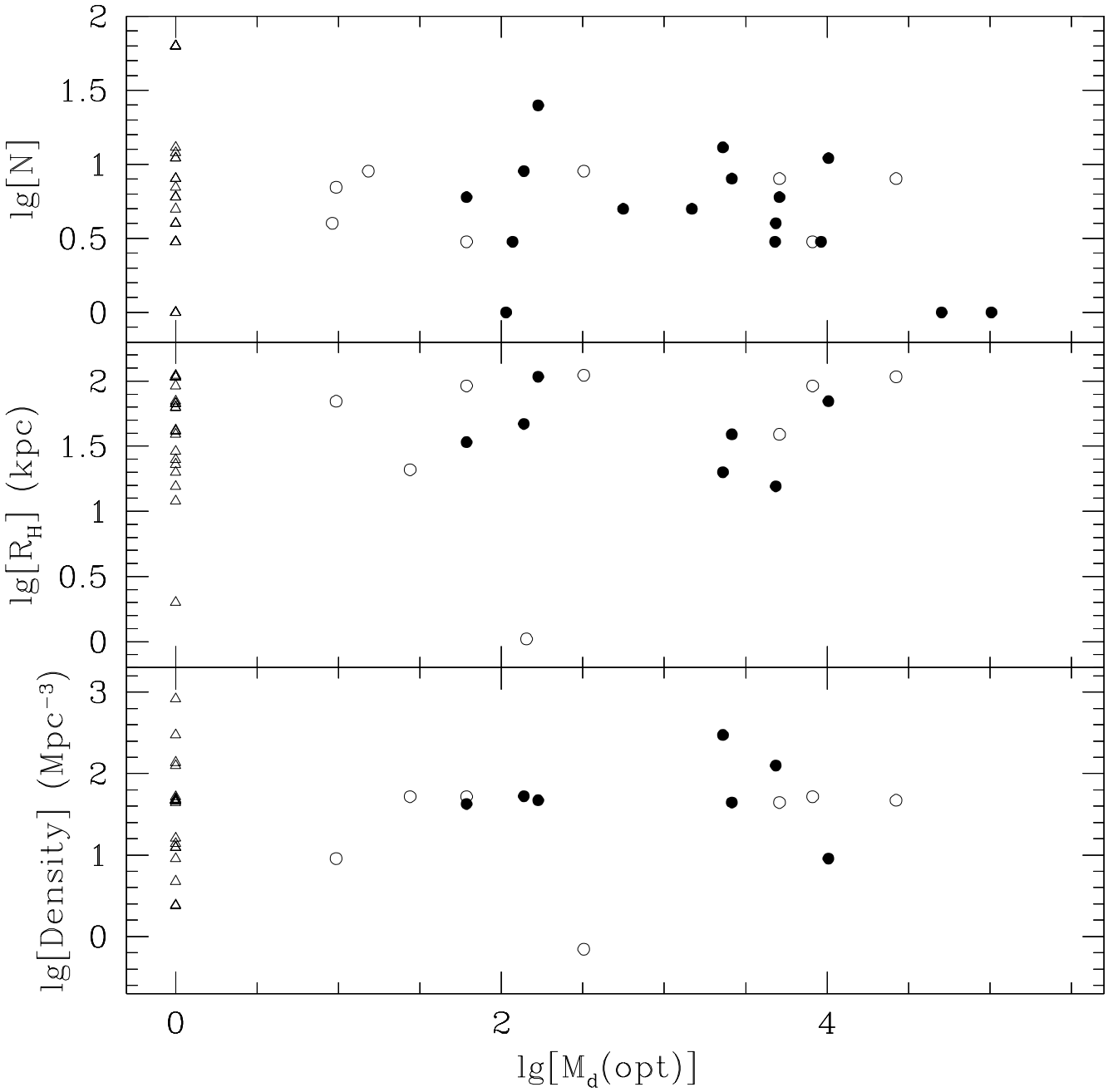

FIG. 10.— The number of group members N, mean harmonic radius R_H, and number density of the group as a function of dust mass for the snapshot sample. Symbols are as in Figure 3. In addition, open triangles denote galaxies with no detectable dust. No correlation is evident between these quantities.

with the presence of clumpy dust, and strongly suggest that the disks and filaments are the source of fuel and gas supply for the radio engines lying at the core of the galaxy. If all galaxies have central BHs (as is very likely) and the presence of dust is higher in galaxies that are active, this implies that galaxies have active duty cycles, and that the central supply of gas and dust is the requisite for the onset of the activity.

The probable relationship between the mass/size of the dusty disks and the central velocity dispersion (§2.3), coupled with a similar correspondence between the latter and the central BH mass, suggests that the mass of the disk is connected with that of the BH. If real, it would imply that activity in early-type galaxies may undergo a process of evolution in which dust is acquired, settles, and provides a channel and fuel reservoir that support the growth and activity of the central massive BH. We note, however, that not all galaxies in which a central BH has been found show visibly detectable dusty disk, and not all galaxies with dusty disk are detected, due to projection effects (van Dokkum & Franx 1995). Thus, the two effects might mitigate each other to some extent.

4. SUMMARY AND CONCLUSIONS

Confirming previous studies, we find that dust is very common in elliptical studies. Although this result has been noted before, our unbiased and volume-limited sample puts such finding on a better footing. There is a strong correspondence between the presence of dust and the detection of radio and far infrared emission. Among those galaxies with visibly detectable dust, a significant correlation is found between the derived mass of the dust and infrared luminosities, especially when only systems with filamentary dust are considered. At the limit of the *IRAS* survey, dusty galaxies are more than 10 times more likely to have 100 μm detection than dustless galaxies, and those with filamentary dust are ~ 4 times more likely to have 100 μm detection than those with dusty disks. This result suggests that the 100 μm radiation most likely comes from filamentary dust which absorbs UV and visible radiation from the surrounding stars and reradiate it in the far-IR. While it is possible to have detection in 100 μm *without* visually detectable dust (e.g., NGC 2549, NGC 3348), the presence of dust makes the detection much more likely.

Galaxies with detectable, clumpy dust are also much more likely to show nuclear activity in the form of radio and line emission than dustless galaxies. The formation of clumpy dust thus appears to be a necessary ingredient for radio and emission-line activity. However, galaxies with dust in small disky morphology are not any more likely to show such activity than those having irregular, filamentary dust. Nearly all dusty disks are well aligned with the major axes of the galaxies in which they reside, while dust filaments seem to be more randomly oriented. If both types of dust have the same origin, then the dust is most likely acquired externally and requires time to settle dynamically. However, there appears to be no correlation between the presence of dust and the ambient galaxy density. Alternatively, the two types of dust may have different origins. A spectroscopic survey to study the dynamics of a well-defined sample of galaxies is needed to confirm the external or internal origin of dust. The possible relationship between the size of the dusty disks with the central velocity dispersion of the galaxy suggests a causal connection between the BH mass and the mass/size of the dusty disk and bulge.

This research is supported by NASA grants 6357 and 8386 from the Space Telescope Science Institute, which is operated by AURA, Inc., under NASA contract NAS5-26555. We thank the referee for a number of very helpful suggestions. We have made use of the CATS database (Verkhodanov et al. 1997) of the Special Astrophysical Observatory, the LEDA database (http://leda.univ-lyon1.fr), and the NASA/IPAC Extragalactic Database (NED), which is operated by the Jet Propulsion Laboratory, California Institute of Technology, under contract with NASA.

REFERENCES

Barnes, J. E., & Hernquist, L. 1996, ApJ, 471, 115
Barnes, J. E., & Hernquist, L. 1998, ApJ, 495, 187
Bennett, S. M., & Moss, C. 1998, A&AS, 132, 55
Bertola, F., & Corsini, E. M. 1999, in *IAU Symp. 186: Galaxy Interactions at Low and High Redshift*, ed. J. E. Barnes & D. B. Sanders, 186, 149
Bettoni, D., & Buson, L. M. 1987, A&AS, 67, 341
Bower, G. A. et al. 1998, ApJ, 492, L111
Bureau, M. et al. 2000, in *Galaxy Disks and Disk Galaxies*, ASP Conference Series, ed. J. G. Funes S. J. & E. M. Corsini, astro-ph/0009332
Buson, L. M., Sadler, E. M., Zeilinger, W. W., Bertin, G., Bertola, F., Danzinger, J., Dejonghe, H., Saglia, R. P., & de Zeeuw, P. T. 1993, A&A, 280, 409
Caldwell, N. 1984, PASP, 96, 287
Calvani, M., Fasano, G., & Franceschini, A. 1989, AJ, 97, 1319
Caon, N., Macchetto, D. & Pastoriza, M. 2000, ApJS, 127, 39
Cardelli, J. A., Clayton, G. C., & Mathis, J. S. 1989, ApJ, 345, 245
Condon, J. J., Cotton, W. D., Greisen, E. W., Yin, Q. F., Perley, R. A., Taylor, G. B., & Broderick, J. J. 1998, AJ, 115, 1693
Davies, R. L., Burstein, D., Dressler, A., Faber, S. M., Lynden-Bell, D., Terlevich, R. J., & Wegner, G. 1987, ApJS, 64, 581
de Koff, S., Best, P., Baum, S. A., Sparks, W., Rottgering, H., Miley, G., Golombek, D., Maccheto, F., & Martel, A. 2000, ApJS, 129, 33
Faber, S. M., & Jackson, R. E. 1976, ApJ, 668, 683
Faber, S. M. et al. 1987, in *Nearly Normal Galaxies*, ed. S. Faber, (New York: Springer), p. 175
Faber, S. M. et al. 1997, AJ, 114, 1771
Ferrarese, L., & Ford, H. C. 1999, ApJ, 515, 583
Ferrarese, L., Ford, H. C., & Jaffe, W. 1996, ApJ, 470, 444
Ferrarese, L., & Merritt, D. 2000, ApJ, 539, L9
Ferrarese, L., van den Bosch, F. C., Ford, H. C., Jaffe, W., & O'Connell, R. W. 1994, AJ, 108, 1598
Ferrari, F., Pastoriza, M. G., Macchetto, F., & Caon, N. 1999, A&AS, 136, 269
Forbes, D. A. 1991, MNRAS, 249, 779
Ford, H. C., Tsvetanov, Z. I., Ferrarese, L., Kriss, G., Jaffe, W., Harms, R. & Dressel, L. 1997, in *Accretion Phenomena and Related Outflows*, IAU Coll. No. 163, ed. D. T. Wickramasinghe, G. V. Bicknell, and L. Ferrario, p. 620
Garcia, A. M. 1993, A&AS, 100, 47
Gebhardt, K. et al. 2000, ApJ, 539, L13
Geller, M. J., & Huchra, J. P. 1983, ApJS, 52, 61
Goudfrooij, P., Hansen, L., Jørgensen, H. E., & Nørgaard-Nielsen, H. U. 1994, A&AS, 105, 341
Goudfrooij, P., & de Jong, T. 1995, A&A, 298, 784
Gonzalez, J. J. 1993, Ph.D. Thesis, University of California, Santa Cruz
Harms, R. J. et al. 1994, ApJ, 435, L35
Ho, L. C., Filippenko, A. V., & Sargent, W. L. W. 1995, ApJS, 98, 477

Ho, L. C., Filippenko, A. V., & Sargent, W. L. W. 1997a, ApJS, 112, 315
Ho, L. C., Filippenko, A. V., & Sargent, W. L. W. 1997b, ApJ, 487, 568
Honma, M. 1999, ApJ, 516, 693
Huchra, J. P., & Burg, R. 1992, ApJ, 393, 90
Huchra, J. P., & Geller, M. J. 1982, ApJ, 257, 423
Jaffe, W., Ford, H. C., O'Connell, R. W., van den Bosch, F. C., & Ferrarese, L. 1994, AJ, 108, 1567
Kannappan, S. J., & Fabricant, D. G. 2000, AJ, 121, 140
Kim, D.-W. 1989, ApJ, 346, 653
Knapp, G. R., Guhathakurta, P., Kim, D. and Jura, M. A. 1989, ApJS, 70, 329
Kollatschny, W., & Fricke, K. J. 1989, A&A, 219, 3
Kormendy, J., & Richstone, D. O. 1995, ARA&A, 33, 581
Kwan, J., & Xie, S. 1992, ApJ, 398, 105
Lauer, T. R. et al. 1995, AJ, 110, 2622
Macchetto, F., Marconi, A., Axon, D. J., Capetti, A., Sparks, W. & Crane, P. 1997, ApJ, 489, 579
Macchetto, F., Pastoriza, M., Caon, N., Sparks, W. B., Giavalisco, M., Bender, R., & Capaccioli, M. 1996, A&AS, 120, 463
Martel, A. R., Turner, N. J., Sparks, W. B., & Baum, S. A. 2000, ApJS, 130, 267
Martini, P., & Pogge, R. W. 1999, AJ, 118, 2646
McElroy, D. B. 1995, ApJS, 100, 105
Merluzzi, P. 1998, A&A, 338, 807
Neilsen, E. H., & Tsvetanov, Z. I. 2000, ApJ, 536, 255
Phillips, M. M., Jenkins, C. R., Dopita, M. A., Sadler, E. M., & Binette, L. 1986, AJ, 91, 1062
Osterbrock, D. E., & de Robertis, M. M. 1985, PASP, 97, 1129
Rest, A., van den Bosch, F. C., Jaffe, W., Tran, H. D., Tsvetanov, Z., Ford, H. C., Davies, J., & Schafer, J. 2001, AJ, in press, astro-ph/0102286 (Paper I)
Roberts, M. S., Hogg, D. E., Bregman, J. N., Forman, W. R., & Jones, C. 1991, ApJS, 75, 751
Sadler, E. M., & Gerhard, O. E. 1985, MNRAS, 214, 177
Shields, J. C. 1991, AJ, 102, 1314
Sparks, W. B., Baum, S. A., Biretta, J., Macchetto, D., & Martel, A. R. 2000, ApJ, 542, 667
Steiman-Cameron, T. Y., & Durisen, R. H. 1988, ApJ, 325, 26
Tohline, J. E., Simonson, G. F., & Caldwell, N. 1982, ApJ, 252, 92
Tomita, A., Aoki, K., Watanabe, M., Takata, T., & Ichikawa, S. 2000, AJ, 120, 123
Trinchieri, G., & di Serego Alighieri, S. 1991, AJ, 101, 1647
Tsai, J. C., & Mathews, W. G. 1996, ApJ, 468, 571
van den Bosch, F. C., Ferrarese, L., Jaffe, W., Ford, H. C., & O'Connell, R. W. 1994, AJ, 108, 1579
van der Marel, R. P. 1999, in *Galaxy Interactions at Low and High Redshifts*, IAU Symp. No. 186, ed. D. B. Sanders, & J. Barnes, (Kluwer:Dordrecht), p. 333
van der Marel, R. P. & van den Bosch, F. 1998, AJ, 116, 2220
Van Dokkum, P. G., & Franx, M. 1995, AJ, 110, 2027
Verdoes Kleijn, G. A., Baum, S. A., de Zeeuw, P. T., & O'Dea, C. P. 1999, AJ, 118, 2592
Verdoes Kleijn, G. A., van der Marel, R. P., Carollo, C. M., & de Zeeuw, P. T. 2000, AJ, 120, 1221
Verkhodanov, O. V., Trushkin S. A., Andernach H., & Chernenkov, V. N. 1997, in *Astronomical Data Analysis Software and Systems VI*, ASP Conf. Ser., ed. G. Hunt & H. E. Payne, 125, 322
Véron-Cetty, M.-P., & Véron, P. 1988, A&A, 204, 28

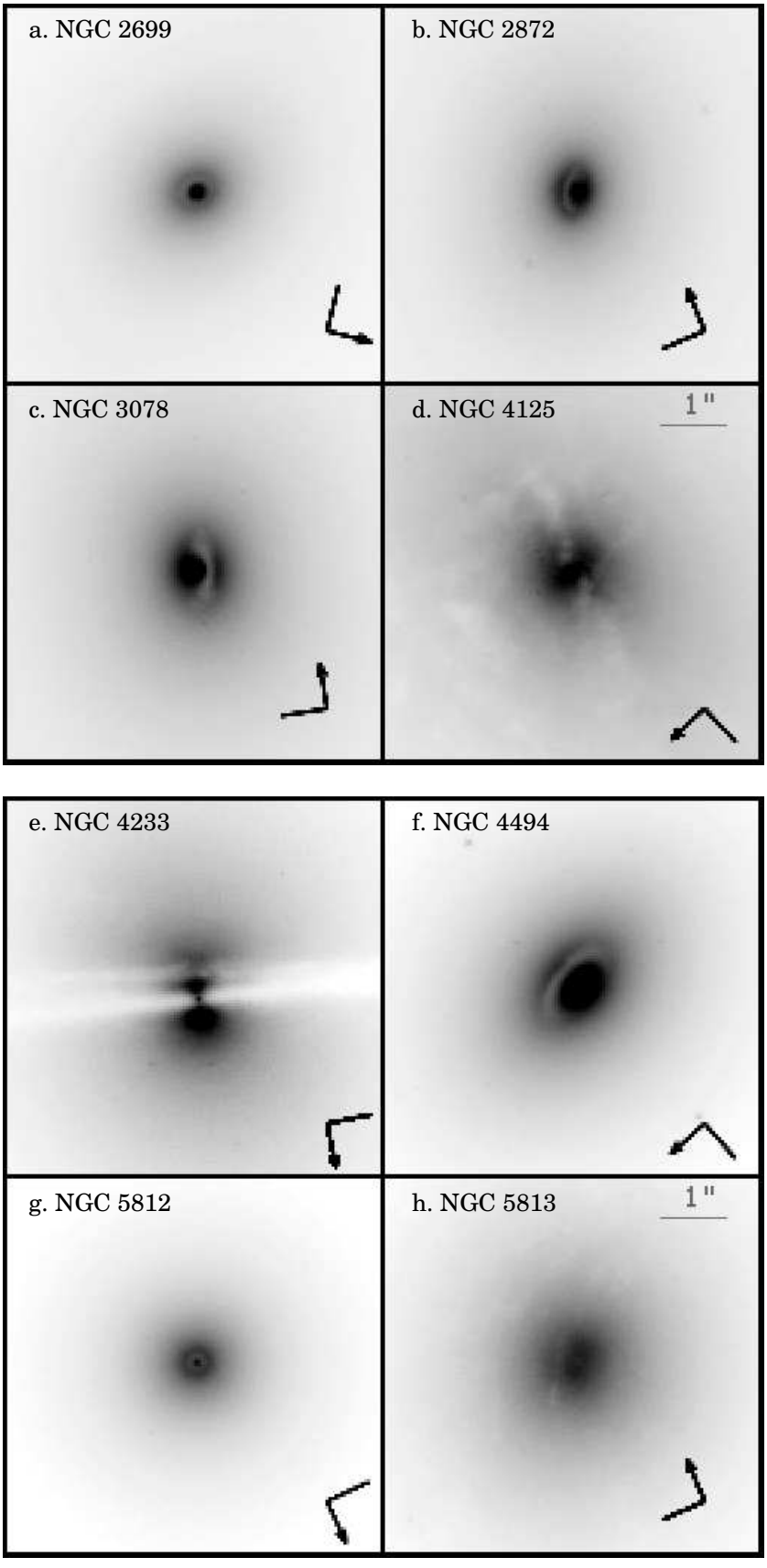
a. NGC 2699
b. NGC 2872
c. NGC 3078
d. NGC 4125
1"
e. NGC 4233
f. NGC 4494
g. NGC 5812
h. NGC 5813
1"

FIG. 1.—

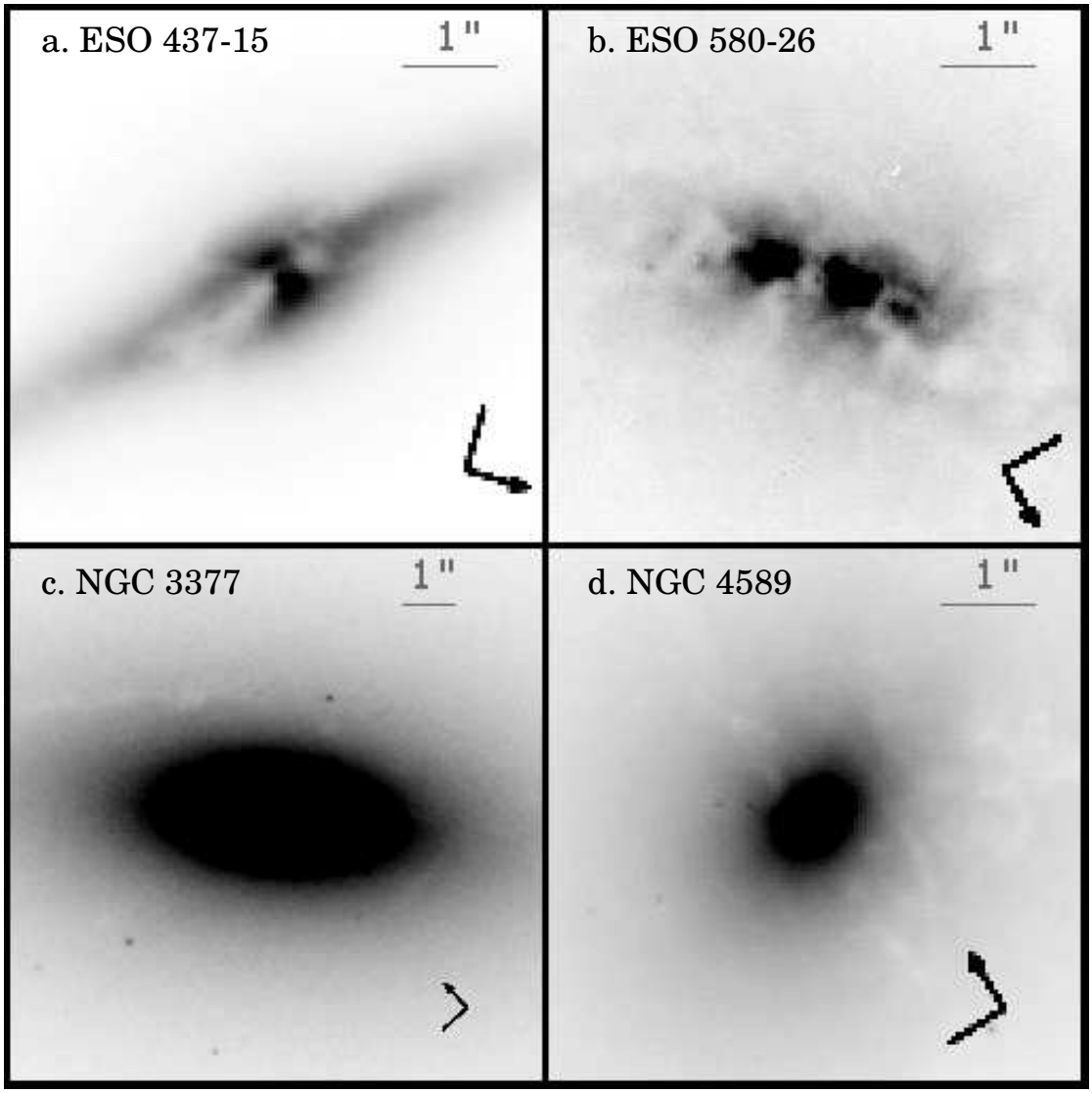

FIG. 2.—

Table 1
Snapshot Sample: General Properties

Name (1)	M_B (2)	B_T (3)	D (4)	Dust (5)	Line Emiss (6)	LGG Group (7)	N (8)	CfA Group (9)	N (10)	R_H (11)	Re (12
ESO 378-20	−19.58	13.17	35.6	0		LGG256	7	...	...	...	
ESO 437-15	−19.41	13.14	32.3	3	N	LGG210	6	...	...	...	BM98
ESO 443-39	−19.41	13.39	36.3	0		LGG328	6	...	...	...	
ESO 447-30	−19.84	12.88	35.0	0		...	..	...	...	...	
ESO 507-27	−19.37	13.56	38.5	0		LGG310	12	...	...	...	
ESO 580-26	−18.12	14.85	39.3	3	L	...	..	...	...	...	OD85
IC 875	−19.17	13.73	37.9	0		...	..	...	2	...	
MCG 11-14-25A	−17.90	15.32	44.2	0		LGG238	3	GH82	6	0.67	
MCG 8-27-18	−18.85	14.36	43.7	0		...	..	...	...	...	
NGC 2549	−19.22	11.76	15.7	0	N	...	1	...	1	0	H97
NGC 2592	−18.92	13.11	25.5	4		...	..	...	3	...	
NGC 2634	−19.99	12.50	31.4	0	N	LGG160	5	HG90	3	0.25	H97
NGC 2699	−18.72	12.97	21.8	4		LGG164	4	...	...	...	
NGC 2778	−19.06	13.06	26.6	0	Y	LGG171	3	GH43	5	0.42	G93
NGC 2824	−19.75	13.92	54.2	3		...	1	...	1	0	
NGC 2872	−20.38	12.54	38.3	4		...	..	H99	2	0.0105	
NGC 2902	−18.97	12.86	23.3	2		LGG174	3	...	...	...	
NGC 2950	−19.93	11.52	19.5	0	N	...	1	...	1	0	H97
NGC 2986	−20.87	11.27	26.8	0	N	...	..	...	2	...	G94
NGC 3065	−19.56	12.69	28.2	4	Y	...	..	...	2	...	BB87, R
NGC 3078	−20.71	11.60	29.0	4	Y	LGG185	9	HG29	4	1.11	TD91
NGC 3193	−19.62	11.64	17.9	0	L2:	LGG194	13	GH58	10	0.20	H95, H9
NGC 3226	−19.11	12.08	17.3	3	L1.9	LGG194	13	GH58	10	0.20	H95, H9
NGC 3266	−19.11	13.18	28.6	0		...	..	GH63	4	0.41	
NGC 3348	−21.23	11.69	38.5	0	Y	LGG224	3	GH69	3	0.67	H95
NGC 3377	−18.89	10.90	9.1	1	Y	LGG217	9	GH68	23	0.47	G93, B0
NGC 3414	−19.64	11.73	18.8	1	L2	LGG227	6	GH71	7	0.34	H95, H9
NGC 3595	−19.69	12.72	30.4	0		...	..	...	2	...	
NGC 3613	−20.75	11.49	28.0	0	N	LGG232	4	GH94	170	0.92	G94, H9
NGC 3640	−20.01	11.03	16.2	0	N	LGG233	6	GH76	7	0.23	H97
NGC 4121	−18.31	13.95	28.3	0		...	1	...	1	0	
NGC 4125	−21.20	10.31	20.1	4	T2	LGG274	3	GH94	170	0.92	H95, H9
NGC 4128	−19.97	12.58	32.4	0		LGG272	3	GH99	14	1.11	
NGC 4168	−20.52	11.83	29.5	2	S1.9:	LGG285	25	GH106	248	1.08	R91, H9
NGC 4233	−19.71	12.64	29.6	4	Y	LGG278	8	GH106	248	1.08	KF89
NGC 4291	−20.00	12.04	25.6	0	N	LGG284	11	GH107	13	0.70	H97
NGC 4365	−20.77	10.21	15.7	0	N	LGG289	63	GH106	248	1.08	S91, TD
NGC 4474	−19.42	12.13	20.4	0		LGG289	63	GH106	248	1.08	
NGC 4478	−19.36	11.93	18.1	0	N	LGG289	63	GH106	248	1.08	G93, H9
NGC 4482	−18.52	13.34	23.6	0		LGG296	11	GH106	248	1.08	
NGC 4494	−20.84	10.41	17.8	4	L2::	LGG294	3	GH94	170	0.92	H95, H9
NGC 4503	−19.44	11.79	17.6	0	N	LGG289	63	GH106	248	1.08	H97
NGC 4564	−19.15	11.67	14.6	0	N	LGG289	63	GH106	248	1.08	G94, H9
NGC 4589	−20.88	11.33	27.6	2	L2	LGG284	11	GH107	13	0.70	G94, H9
NGC 4621	−18.50	10.41	6.0	0	N	...	..	GH106	248	1.08	H97
NGC 4648	−19.09	12.60	21.8	4	N	LGG303	7	GH107	13	0.70	H97
NGC 5017	−19.19	13.25	30.8	4		LGG338	9	...	...	...	
NGC 5077	−20.63	12.03	34.0	2	L1.9	LGG343	3	...	...	...	M96, H9
NGC 5173	−19.52	13.07	32.8	3	Y	LGG352	4	H99	2	0.156	BB87
NGC 5198	−20.24	12.42	34.1	0	Y	LGG352	4	H99	2	0.156	R91
NGC 5283	−18.93	14.13	40.8	3	S2	...	1	...	1	0	HB92

TABLE 1—*Continued*

Name (1)	M_B (2)	B_T (3)	D (4)	Dust (5)	Line Emiss (6)	LGG Group (7)	N (8)	CfA Group (9)	N (10)	R_H (11)	Ref (12)
NGC 5308	−20.13	11.99	26.6	0	N	LGG360	8	GH122	13	0.63	H97
NGC 5370	−19.45	13.63	41.3	0		...	..	GH122	13	0.63	
NGC 5557	−21.52	11.62	42.5	0	N	LGG378	3	GH141	13	0.02	H97
NGC 5576	−20.00	11.41	19.1	0	N	LGG379	6	GH139	6	0.12	H97
NGC 5796	−20.38	12.43	36.5	1	N	LGG390	3	...	...	...	R91
NGC 5812	−20.10	11.86	24.6	4	Y	...	..	H99	2	0.209	G93, M96
NGC 5813	−20.85	11.11	24.6	4	L2:	LGG393	8	GH150	11	0.39	G93, H95, H97
NGC 5831	−19.59	12.06	21.4	0	Y	LGG393	8	GH150	11	0.39	G93, M96
NGC 5846	−21.10	10.74	23.3	3	Y	LGG393	8	GH150	11	0.39	BB87, B93, G93
NGC 5898	−20.30	11.80	26.3	1	Y	LGG398	5	...	...	...	R91, M96
NGC 5903	−20.85	11.58	30.5	1	Y	LGG398	5	...	...	...	M96
NGC 5982	−21.32	11.65	39.3	0	L2::	LGG402	4	GH158	5	0.29	H95, H97
NGC 6278	−19.70	13.15	37.1	0		LGG409	3	...	...	...	
UGC 4551	−18.77	13.09	23.6	0		...	1	...	1	0	
UGC 4587	−19.54	13.49	40.3	1		...	1	...	1	0	
UGC 6062	−18.82	13.74	32.7	0		...	1	...	1	0	

Note. — Column (1): Name of the galaxy.
Column (2): Absolute B-band magnitude, from Paper I.
Column (3): Total apparent B-band magnitude, from Paper I.
Column (4): Distance in Mpc, from paper I.
Column (5): Dust level: 0 = No dust, 1 = Filamentary low, 2 = Filamentary medium, 3 = Filamentary high, 4 = dusty disk.
Column (6): Presence of line emission: Empty entry denotes no observation or no information from literature; N = no line emissio detected, Y = emission line detected. Wherever the type of activity has been determined by Ho et al. (1997a), this information given (LINER: L1.9, L2; Transition object: T2; Seyfert: S1.9, S2). Colons denote uncertainty.
Column (7): Lyon Group of Galaxies (LGG) group number from Garcia (1993).
Column (8): Number of members in LGG group; = 1 if appeared isolated.
Column (9): CfA group number from Geller & Huchra (1983) and Huchra & Geller (1982), or H99 denoting that the galaxy is member of a galaxy pair in Honma (1999).
Column (10): Number of members in CfA group, or if = 2, indicating that the galaxy is in an interacting pair or having anoth companion; = 1 if appeared isolated.
Column (11): Mean harmonic radius of the group in Mpc from Geller & Huchra (1983) and Huchra & Geller (1982); if a binary, t separation between the pair.
Column (12): References for emission lines: B93=Buson et al. (1993); B00=Bureau et al. (2000); BB87=Bettoni & Buson (1987 BM98=Bennett & Moss (1998); G93=Gonzalez (1993); G94=Goudfrooij et al. (1994); H95=Ho et al. (1995); H97=Ho et al. (1997a HB92=Huchra & Burg (1992); KF89=Kollatschny & Fricke (1989); OD85=Osterbrock & de Robertis (1985); M96=Macchetto et a (1996); R91=Roberts et al. (1991); S91=Shields (1991); TD91=Trinchieri & di Serego Alighieri (1991).

Table 2
Snapshot Sample: Dust Properties

Name (1)	Morph (2)	d (3)	i (4)	$\langle A_V \rangle$ (5)	M_d(opt) (6)	PA_g (7)	PA_d (8)	$\lvert\Delta PA\rvert$ (9)
ESO 437-15	F3			0.17	3.70	41	42	1
ESO 580-26	F3			0.21	4.42	41	30	11
NGC 2592	D	0.6	34	0.093	1.53	50	55	5
NGC 2699	D	0.6	40	0.029	0.96	45	45	0
NGC 2824	F3			0.16	5.00	−20	145	15
NGC 2872	D	0.9	63	0.20	2.15	−30	155	5
NGC 2902	F2			0.061	2.06	10	112	78
NGC 3065	D	0.5	···	0.10	1.28	−60	···	···
NGC 3078	D	1.4	75	0.33	2.50	−01	175	4
NGC 3226	F3			0.13	3.35	43	15	28
NGC 3377	F1			0.047	2.13	41	50	9
NGC 3414	F1			0.034	1.78	01	93	88
NGC 4125	D	3.3	~ 90	0.11	3.90	−98	72	10
NGC 4168	F2			0.035	2.22	−52	105	23
NGC 4233	D	5.4	~ 90	0.52	4.42	25	77	52
NGC 4494	D	1.6	50	0.20	1.78	01	10	9
NGC 4589	F2			0.073	4.00	−88	00	88
NGC 4648	D	0.4	···	0.10	0.98	65	···	···
NGC 5017	D	0.5	~ 0	0.029	1.18	32	···	···
NGC 5077	F2			0.048	3.96	09	102	87
NGC 5173	F3			0.055	3.68	−79	115	14
NGC 5283	F3			0.173	4.70	−85	109	14
NGC 5796	F1			0.067	3.67	−76	16	88
NGC 5812	D	0.4	~ 10	0.11	1.43	60	···	···
NGC 5813	D	1.4	~ 65	0.083	3.70	−39	150	9
NGC 5846	F3			0.030	3.41	−101	52	27
NGC 5898	F1			0.035	2.74	−70	00	70
NGC 5903	F1			0.063	3.16	−14	−04	10
UGC 4587	F1			0.029	2.02	07	05	2

Note. — Column (1): Galaxy name.
Column (2): Morphology of the dust features: F = filaments, with a number denoting the level of dust as in Paper I; D = dusty disk.
Column (3): Diameter of the dusty disk in arcsec.
Column (4): Inclination of the dusty disk in degrees, derived from the ellipticity and the assumption that the disk is intrinsically circular.
Column (5): Mean visual extinction of the dust features in magnitude.
Column (6): Dust mass in units of log $M_\odot$ derived from visual extinction of the visible dust features.
Column (7): PA of the major axis of the galaxy measured at $10''$.
Column (8): PA of the major axis of the main dust structure.
Column (9): Absolute value of the difference $PA_g - PA_d$.

TABLE 3
DUST MASS COMPARISON TO PREVIOUS STUDIES

Galaxy	This work	vD&F95[a]	Tom00[b]
NGC 3377	4.2	···	4.8
NGC 4494	3.9	4.0	5.0
NGC 4589	6.1	5.8	7.0
NGC 5813	5.8	4.8	6.5

Note. — The table lists gas mass in logarithmic solar mass units. Previous values were converted using distances adopted in this paper listed in Table 1. A gas-to-dust ratio of 130 has been assumed.

[a]van Dokkum & Franx (1995)

[b]Tomita et al. (2000)

Table 4
Snapshot Sample: Radio and Infrared Properties

	S_{1400}	σ_{1400}	S_{60}	σ_{60}	S_{100}	σ_{100}	S_{60}/S_{100}	T_d[a]	$M_d(IRAS)$[b]
ESO 437-15	0.0035	0.0006	0.83	0.068	1.16	0.094	0.72	44.5	5.18
ESO 447-30	···	···	0.30	0.042	1.44	0.100	0.21	27	6.27
ESO 580-26	0.0037	0.0007	0.98	0.074	1.83	0.110	0.54	39.5	5.73
NGC 2549	···	···	0.26	0.048	0.37	0.131	0.70	44	4.07
NGC 2634[c]	···	···	0.28	0.032	0.98	0.165	0.29	30	5.77
NGC 2778	···	···	0.00	0.041	0.51	0.096	0.00	30	5.34
NGC 2824	0.0093	0.0005	0.94	0.074	1.51	0.100	0.62	42	5.83
NGC 2872	0.0074	0.0026							
NGC 2902	···	···	0.16	0.040	1.04	0.183	0.15	24	6.06
NGC 2950	···	···	0.16	0.033	0.20	0.115	0.80	48	3.87
NGC 2986	···	···	0.00	0.025	0.40	0.123	0.00	30	5.25
NGC 3065[c]	0.0045	0.0006	1.51	0.025	2.00	0.100	0.76	46	5.25
NGC 3078	0.3138	0.0109							
NGC 3226	0.0033	0.0005							
NGC 3348	0.0083	0.0005	0.13	0.029	0.30	0.139	0.43	35	5.14
NGC 3377	···	···	0.14	0.045	0.35	0.065	0.40	34.5	3.98
NGC 3414	0.0047	0.0005	0.25	0.025	0.56	0.185	0.45	36	4.73
NGC 4125	···	···	0.70	0.044	1.67	0.069	0.42	35	5.32
NGC 4168	0.0060	0.0015	0.00	0.036	0.66	0.157	0.00	30	5.55
NGC 4233	0.0034	0.0006	0.19	0.037	0.48	0.087	0.40	34.5	5.14
NGC 4365	···	···	0.00	0.044	0.65	0.131	0.00	30	4.99
NGC 4494	···	···	0.19	0.049	0.00	0.170	....	30	4.90
NGC 4564	$\lesssim 0.0025$								
NGC 4589	0.0378	0.0015	0.20	0.031	0.66	0.153	0.30	31	5.42
NGC 5077	0.1608	0.0057							
NGC 5173	0.0032	0.0006	0.35	0.042	0.53	0.159	0.66	43.5	4.88
NGC 5198	0.0040	0.0006							
NGC 5283	0.0134	0.0004							
NGC 5576	···	···	0.09	0.027	0.21	0.278	0.43	35	4.37
NGC 5796	0.1100	0.0044							
NGC 5812	$\lesssim 0.002$								
NGC 5813	0.0158	0.0011							
NGC 5846	0.0221	0.0014							
NGC 5898	···	···	0.13	0.036	0.23	0.072	0.56	40	4.46
NGC 5903	0.0318	0.0021							
NGC 5982	···	···	0.00	0.033	0.37	0.035	0.00	30	5.54
NGC 6278	···	···	0.00	0.023	0.32	0.100	0.00	30	5.43
UGC 4587	···	···	0.14	0.028	0.94	0.061	0.15	24	6.50

Note. — S_{1400} (σ_{1400}), S_{60} (σ_{60}), S_{100} (σ_{100}) are the 1400 MHz, 60μm and 100μm flux densities (and their associated errors) in Jy, respectively.

[a]Dust temperature in Kelvin, derived from color ratio S_{60}/S_{100}. When S_{60}/S_{100} is not available, a temperature of 30K is assumed.

[b]Dust mass in units of log $M_\odot$ derived from *IRAS* flux densities and dust color temperature.

[c]Infrared fluxes may likely be contaminated with emission from nearby sources (Knapp et al. 1989).

Table 5
Pearson Correlation Coefficients

Relationship	N	r	p
log L_{IR60} – log M_d(opt)	13[a]	0.76[a]	0.0032[a]
	10	0.80	0.0075
log L_{IR100} – log M_d(opt)	13[a]	0.57[a]	0.044[a]
	11	0.63	0.040
log L_{rad} – log M_d(opt)	18	0.21	0.41
	13	0.43	0.15
log L_{IR60} – M_B	20	0.14	0.54
	16	0.10	0.71
log L_{IR100} – M_B	25	0.080	0.70
	22	0.094	0.68
log L_{rad} – M_B	20	−0.44	0.051
	15	−0.42	0.12
M_B – log M_d(opt)	29	−0.15	0.44
	11[b]	−0.83[b]	0.003[b]

Note. — For each pair of variables, the number of data points (N), the linear correlation coefficient (r), and the probability of the null hypothesis (no correlation, p) are shown in the first line for all galaxies with dusty disks and filamentary dust. The second line shows the results for galaxies with filamentary dust only, except for M_B – log M_d(opt), where it shows the coefficients for galaxies with dusty disks.

[a]Excluding NGC 3065

[b]Excluding NGC 4233

Table 6
Detection Rates

	Dusty Disks (12, 15)	Fil Dust (17, 16)	All Dust (29, 31)	No Dust (38, 9)	All Gal (67, 40)
EL – snapshot	8 7 88	14 12 86	22 19 86	21 6 28	43 25 58
– *IRAS*	14 12 86	16 12 75	30 24 80	8 2 25	38 26 68
Radio – snapshot	12 6 50	17 13 76	29 19 66	38 3 8	67 22 33
– *IRAS*	13 8 62	16 8 50	29 16 55	9 2 22	38 18 47
Far-IR[a] – snapshot	10 4 40	15 11 73	25 15 60	37 11 30	62 26 42
Group – snapshot	12 12 100	16 13 81	28 25 89	36 31 86	64 56 88

Note. — Detection rate of emission lines (EL), radio emission from NVSS, far-IR emission from *IRAS* survey, and being in a group/cluster/binary pair. For each group, the first number indicates the total number of galaxies with available data, the second number denotes the number of galaxies with detections, and the last number gives the percentage relative to the number of galaxies with available data within that group. Values for the snapshot sample are given in the first line, and for the *IRAS* sample in the second line. The first and second number in parentheses in the heading give the total number of galaxies in each group for the snapshot and *IRAS* sample, respectively.

[a]By definition, the far-IR detection rate for the *IRAS* sample is 100%.

TABLE 7
IRAS SAMPLE

Name (1)	v (2)	B_T (3)	Dust (4)	Radio (5)	Line Emiss (6)	Ref (7)
ESO 208-G021	1037	12.19	4	···	Y	P86
ESO 358-G059	1007	13.99	0	N		
IC 1459	1691	10.97	4	Y	Y	B93, R91, G94
NGC 205(M110)	−241	8.92	1	N	N	H97
NGC 404	−48	11.21	3	Y	L2	R91, H97
NGC 584	1875	11.44	1	N	Y	M96
NGC 821	1718	11.67	0	N	N	G93, H97
NGC 1052	1470	11.41	2	Y	L1.9	H97
NGC 1339	1392	12.51	0	N	N	R91
NGC 1351	1511	12.46	0	N	N	P86
NGC 1399	1425	10.55	0	Y	Y	G94, M96
NGC 1400	558	11.92	2	Y	N	M96
NGC 1404	1947	11.92	1	Y	N	G94
NGC 1439	1670	12.27	4	N	N	R91
NGC 2768	1339	10.84	4	Y	L2	H97
NGC 2778[a]	2032	13.35	0	N	Y	G93
NGC 2974	2072	11.87	3	Y	Y	R91
NGC 2986[a]	2329	11.72	0	N	N	G94
NGC 3156	1118	13.07	2	N	Y	BB87
NGC 3377[a]	692	11.24	1	N	Y	G93, B00
NGC 3610	1787	11.70	3	N	Y	G94
NGC 4125[a]	1356	10.65	4	N	T2	H97
NGC 4168[a]	2284	12.11	2	Y	S1.9	R91, H97
NGC 4261	2210	11.14	4	Y	L2	G93, H97
NGC 4278	649	11.09	3	Y	L1.9	R91, H97
NGC 4365[a]	1240	10.52	0	N	N	S91, TD91, H97
NGC 4374(M84)	1000	10.09	4	Y	L2	H97
NGC 4406(M86)	−227	9.83	4	N	N	H97
NGC 4476	1978	13.01	3	N	N	R91
NGC 4486(M87)	1282	9.59	4	Y	L2	H97
NGC 4552(M89)	321	10.73	4	Y	T2:	H97
NGC 4589[a]	1980	11.69	2	Y	L2	G94, H97
NGC 4649(M60)	1413	9.81	0	Y	N	H97
NGC 4697	1236	10.14	4	N	Y	G93
NGC 4742	1270	12.12	3	N	Y	R91
NGC 5128(Cen A)	547	7.84	4	Y	Y	P86
NGC 5322	1915	11.14	4	Y	L2::	H97
NGC 5845	1450	13.50	4	N		
NGC 5898[a]	2209	12.49	1	N	Y	R91, M96
NGC 6861	2819	12.12	4	···	Y	P86

Note. — Column (1): Name of the galaxy.
Column (2): Heliocentric velocity in km s^{-1}.
Column (3): Total apparent B-band magnitude.
Column (4): Dust level as in Table 1.
Column (5): Radio detection at 1.4 Ghz from NVSS or FIRST survey.
Column (6): Presence of line emission.
Column (7): References for emission lines as in Table 1; also P86=Phillips et al. (1986).

[a]Also in the snapshot sample.